RSC Advances

Luminescent properties of a pink emitting persistent phosphor Pr3+-doped La3GaGe5O16

Journal:	*RSC Advances*
Manuscript ID:	RA-ART-03-2015-005116
Article Type:	Paper
Date Submitted by the Author:	23-Mar-2015
Complete List of Authors:	Zhang, Shaoan; Guangdong University of Technology, School of Physics and Optoelectronic Engineering Hu, Yihua; Guangdong University of Technology, School of Physics and Optoelectronic Engineering Chen, Li; Guangdong University of Technology, School of Physics and Optoelectronic Engineering Ju, Guifang; Guangdong University of Technology, School of Physics and Optoelectronic Engineering Wang, Tao; Guangdong University of Technology, School of Physics and Optoelectronic Engineering Wang, Zhonghua; Guangdong University of Technology, School of Physics and Optoelectronic Engineering

Luminescent properties of a pink emitting persistent phosphor Pr^{3+}-doped $La_3GaGe_5O_{16}$

Shaoan Zhang, Yihua Hu*, Li Chen, GuiFang Ju , Tao Wang, and Zhonghua Wang

School of Physics and Optoelectronic Engineering, Guangdong University of Technology, Waihuan Xi Road, No.100, Guangzhou 510006, People's Republic of China.

Abstract:

This pink persistent phosphor $La_3GaGe_5O_{16}:Pr^{3+}$ was prepared successfully via the traditional solid state reaction method. In this paper, $La_3GaGe_5O_{16}$ host is proved to be a new self-activated luminescent host lattice on a basis of the excitation and emission spectra. $La_3GaGe_5O_{16}$ host gives a blue emission under excitation with 260 nm. Two parts line peaks of $La_{2.99}GaGe_5O_{16}:0.01Pr^{3+}$ in the emission spectra arise from $^3P_0 \rightarrow {}^3H_4$ transition in the blue region and $^3P_0 \rightarrow {}^3H_6$ in the red region, respectively. However, concentration quenching of Pr^{3+} in $La_3GaGe_5O_{16}:Pr^{3+}$ occurs at a low content of 0.02 in this work, which is mainly due to the dipole-dipole interaction. $La_3GaGe_5O_{16}:Pr^{3+}$ phosphors present pink long persistent luminescence after the short UV-irradiation. The optical concentration of Pr^{3+} for the long persistent luminescence in $La_3GaGe_5O_{16}$ host are experimentally about 0.01. The long persistent luminescence of $La_3GaGe_5O_{16}:Pr^{3+}$ is discussed in accordance with the afterglow decays and thermoluminescence analysis. A model is proposed based on the experimental results to explain the mechanisms of the photoluminescence and afterglow phenomenon.

Keywords: Photoluminescence; Pink afterglow; Optical materials

* Corresponding author. Tel.:+86-020-39322262;

Fax: +86-020-39322265

E-mail address: huyh@gdut.edu.cn (Yihua Hu)

1. Introduction

phosphorescence or long afterglow is an interesting optical phenomenon, which is a special case of thermally stimulated luminescence after stopping excitation. Compared to the fluorescence phenomenon, phosphorescence can last for several minutes or hours after the removal of the activated light source, which is much longer than that of fluorescence [1-2]. So the practical application difference between fluorescence and phosphorescence are obvious. On the one hand, fluorescence phosphors usually attracted extensive research interest for their possible application to white LEDs or solar cells [3-5]. On the other hand, phosphorescence particles are commercialized as night or dark environment vision materials for their wide application, *e.g.* , such as emergency escape routes and exit signs, optical energy media, thermal sensors [6-8]. Besides the traditional applications, new fields of interest emerged in medical field such as cancer photodynamic therapy, cancer diagnoses and *in vivo* imaging [9-10].

The first application of persistent luminescence came in the middle of 1990s with ZnS:Cu, Co for making watch dials [11]. In 1996, Matsuzawa *et al.* reported a new persistent luminescence materials ($SrAl_2O_3:Eu^{2+}$, Dy^{3+}) which can emit in visible for 10h after ceasing the irradiation and gave us a new benchmark for the performance of persistent luminescence materials [12]. Since then, this new finding boosted the research on the persistent luminescence phosphors and many efficient persistent luminescence materials based on stable aluminate and silicate materials were discovered, i.e., $CaAl_2O_3:Eu^{2+}$, Dy^{3+}[13], $Sr_4Al_{14}O_{25}:Eu^{2+}$, Dy^{3+}[14], and $Sr_2MgSi_2O_7:Eu^{2+}$, Dy^{3+} [15]. It is worth encouraging that the yellow-green, green-blue, and blue persistent phosphors with high brightness and long afterglow time have been available in the commercial market [12-15]. However, orange to red persistent phosphors can't still meet commercial purpose in spite that

much effort had been devoted to the research of orange to red persistent phosphors. In the early time, red persistent phosphors were mainly prepared by rare earth ions activated sulfides but they are instable [16]. $Y_2O_2S:Eu^{3+},Ti^{4+}$, Mg^{2+} red persistent phosphor was reported to show better stability and longer red afterglow time (above 5h) [17]. Generally, such oxysulfides were obtained under weak reducing atmosphere which requires better equipment and complicated technique. Moreover, harm gas released in the process of synthesis. At recent years, a few orange-red persistent phosphors have been reported such as $MWO_4:Eu^{3+}/Sm^{3+}$(M=Ca, Sr and Ba) [18-20], $Ca_2Si_5N_8:Eu^{2+}$[21], $Ca_2SnO4:Sm^{3+}$ [22], $Sr_3Al_2O_5Cl_2:Eu^{2+},Tm^{3+}$ [23], *etc*. However, it is still far away from the expected target for orange-red persistent phosphors due to their unsatisfactory afterglow intensity or time. Therefore, it is essential to explore a more excellent orange to red persistent phosphor.

Except for the rare earths Eu^{2+}, Eu^{3+} and Sm^{3+} doped activators, Pr^{3+} ion is also a promising dopants for the orange to red persistent phosphor. Plenty of Pr^{3+}-doped phosphors had been reported, such as $CaTiO_3:Pr^{3+}$ [24], $Ca_2Zn_4Ti1_6O_{38}:Pr^{3+}$[25], $NaNbO_3:Pr^{3+}$ [26], YPO_4: Pr, Ln [27], *etc*. These phosphors present a red afterglow luminescence and give us a hint to explore the ideal red afterglow phosphor. In this work, we select the Pr^{3+} ions as the activators and the gallogermanates ($La_3GaGe_5O_{16}$) as the target host is due to its unique crystal structure. G. Adiwidjaja firstly reported the gallogermanates of lanthanum compound and revealed its chemical composition and detailed crystal structure [28]. The basic structural units are composed of [GeO_6] octahedron, [GeO_4] tetrahedron and [GaO4] tetrahedron. Each [GeO_6] octahedron is connected with six tetrahedron via common corners; every tetrahedron is linked to two octahedron forming chains of composition [$Ge(Ga,GeO_4)_3$] parallel [100]. In the b, c-plane the chains are connected by

[Ge_2O_8] groups which consist of two-edge-linked pseudo-tetragonal GeO_5 pyramids to a three dimensional framework structure with channels parallel [100]. Recently, only Xia et al. reported the multi-color emission evolution and energy transfer behavior of $La_3GaGe_5O_{16}:Tb^{3+},Eu^{3+}$ phosphors and near-infrared luminescence of $La_3GaGe_5O_{16}:Cr^{3+}$ phosphors [29-30]. As far as we know, there is still no report about the photoluminescence and persistent properties of $La_3GaGe_5O_{16}:Pr^{3+}$. In this paper, $La_3GaGe_5O_{16}:Pr^{3+}$ phosphor can show a pink persistent luminescence for several minutes. The concentration quenching, the afterglow decays and the afterglow mechanism have been investigated. All the results indicate that there might be some promising potential practical application for $La_3GaGe_5O_{16}:Pr^{3+}$ phosphor in the traditional domain.

2. Experimental procedures

2.1 Synthesis

The samples were prepared by a simple solid state reaction. La_2O_3(99.99%), Ga_2O_3 (99.99%), GeO_2 (99.99%) and Pr_6O_{11} (99.99%) were used as starting materials. After the raw materials were weighed according to the composition of $La_{3-x}GaGe_5O_{16}:Pr^{3+}:xPr^{3+}$($x$=0, 0.005, 0.01, 0.02, 0.03, 0.04, 0.05 and 0.07, etc), the powders were mixed and milled thoroughly for 1h in an agate mortar and prefired at 900℃ for 8h in air. After ground again, the mixtures were sintered at 1300℃ for 12h. After being cooled down to room temperature naturally, the as-prepared powder samples were obtained.

2.2. Characterization of samples

The phase purity of the prepared phosphors was measured by an X-ray diffractometer with Cu Ka radiation (wavelength =0.15406 nm) at 36 kV tube voltage and 20 mA tube current.

Diffuse reflection spectrum was obtained by an ultraviolet (UV)-vis spectrophotometer (Shimadzu UV-2450) using a $BaSO_4$ as a reference; The excitation and emission spectra of all the samples were measured by a Hitachi F-7000 Fluorescence Spectrophotometer equipped with a 150 W xenon lamp as excitation source. The persistent luminescence spectrum was also measured using the spectrophotometer by shutting off the Xe lamp. The decay curves were measured by a GFZF-2A single-photo-counter system. The thermoluminescence (TL) spectrum was measured with a FJ-427A1 thermoluminescence meter. Prior to the persistent luminescence spectra, decay curve and glow curve measurements, the samples were excited for 1 min by a 15 W low-pressure mercury discharge lamp (254 nm). For the glow curve measurements, the heating rate was 1℃/s and the range of the measurement is from room temperature to 300℃. A delay for 1 min was used between the irradiation and measurement. All measurements were carried out at room temperature except for the TL spectrum.

3. Results and discussion

3.1. Phase Characterization

The XRD patterns for all samples were examined to characterize the phase purity and crystallinity of the as-prepared powder samples. Figure 1 shows the XRD pattern of the samples $La_3GaGe_5O_{14}$ host and $La_{3-x}GaGe_5O_{14}$:xPr^{3+}(x=0.005, 0.01, 0.02 and 0.04) along with ICSD card 50521 at the bottom. Evidently, all diffraction peaks are good agreement with the standard data of $La_3GaGe_5O_{14}$ (ICSD#50521). No other impurity phase can be found, indicating that the obtained samples are single phase and the doped Pr^{3+} ions are successfully dissolved into the $La_3GaGe_5O_{14}$ host lattice while maintaining the crystal structure intact. When Pr^{3+} is doped into the this host, it tends to substitute for the lanthanum rather than germanium or gallium sites as a result of matched

size and charge [note: for Pr^{3+} with coordination number(CN) of 8, R_{Pr3+}=1.126Å, CN=8; R_{La3+}=1.160Å, CN=8; R_{Ga3+}=0.47Å, CN=4;R_{Ge4+}=0.53Å, CN=6].

3.2 Photoluminescence Properties

Figure 2a displays the diffuse reflectance spectra of $La_3GaGe_5O_{16}$ host and $La_3GaGe_5O_{16}$:0.01Pr^{3+} sample. The diffuse reflectance spectrum of $La_3GaGe_5O_{16}$ host exhibits a plateau of high reflectivity in the wavelength range of 350-700 nm and starts to decrease notably from 200 to 350 nm which is caused by the host absorption. Compared to the host, the Pr^{3+} doped sample presents much more absorption in the range of 200 to 350 nm, which is attributed to the contribution of host absorption and the Pr^{3+} 4*f*→5*d* transitions. Figure 2b gives the excitation and emission spectra of undoped $La_3GaGe_5O_{16}$ sample in the spectral range from 200 to 700 nm. For undoped $La_3GaGe_5O_{16}$ sample, only one broad band located at 260 nm can be observed when monitored at 460 nm in Figure 2b. This might be assigned to the host absorption, which is in good agreement with the diffuse reflectance spectrum. In the emission spectrum of $La_3GaGe_5O_{16}$ host, there is a primary broad band peaking at 460 nm under excitation with 260 nm in Figure 2. The broad band ranging from 370 to 600 nm is attributed to the recombination of self-trapped excitons (STEs) [31-33], which the electrons in the valence band (VB) absorb photons and get excited to some localized sensitizing centers correlated with surface states in the forbidden gap, associating with the electron polarons and holes but not directly to the conduction band (CB). [34]

The STE might be closely related to the oxygen or germanium vacancy deficiency in host. The melting points of raw materials La_2O_3, Ga_2O_3 and GeO_2 are 2315, 1115 and 1740℃, respectively. when prepared at 1300 ℃ for 12 h, the loss of GeO_2 to gas is unavoidable. So, the vacancy deficiency could be produced during the high-temperature synthesis processes in $La_3GaGe_5O_{16}$

host. The photoluminescence properties of the La_3GaGe_5O16 host are still not reported up to now. We can conclude that $La_3GaGe_5O_{16}$ is a new self-activated luminescent host lattice on a basis of the above excitation and emission spectra.

The excitation spectrum of $La_{2.99}GaGe_5O_{16}$:0.01Pr^{3+}, as shown in Fig. 3(a), consists of a asymmetric broad band and some narrow lines when monitoring the transition of the $^1D_2 \rightarrow {}^3H_4$ located at 612 nm. The broad band can be attributed to the contribution of host absorption and the Pr^{3+} 4*f*→5*d* transitions; in addition, some weak and narrow lines are defected, which arise from the interconfiguratonal 4*f*→4*f* transitions [24]. A striking feature in the excitation spectrum is the weakness of the interconfiguratonal 4*f*→4*f* transitions when compared to the 4*f*→5*d* transition since the former is the spin and parity forbidden, however, the latter is parity allowed.

The emission spectrum of $La_{2.99}GaGe_5O_{16}$:0.01Pr^{3+} in Fig. 3(b) consists of a series of the sharp characteristic emission peaks of Pr^{3+} corresponding to the 4*f*→4*f* transitions within its interconfiguratonal $4f^3$ configuration. Two series dominated emission peaks can be assigned to the $^3P_0 \rightarrow {}^3H_4$ and $^1D_2 \rightarrow {}^3H_4$ transitions of Pr^{3+} in the wavelength range of 470-510 nm and 580-620 nm, respectively. The other recessive emission peaks can be attributed to the $^3P_0 \rightarrow {}^3H_5$, $^3P_0 \rightarrow {}^3H_6$ and $^1D_2 \rightarrow {}^3H_6$ transitions of Pr^{3+}, respectively.

Figure 4 presents the integrated intensity of Pr^{3+} as a function of its doping concentrations. As the result shows, the integrated intensity of Pr^{3+} increases with the increasing concentration of Pr^{3+} ions, the luminescent intensity of Pr^{3+} reaches the highest intensity when the doping concentration of Pr^{3+} increases to 0.02 and then decreases. Thus the optical doping concentration of Pr^{3+} is determined to be about 0.02 and the quenching concentration also can be obtained. Generally, there are two different types that can cause the phenomenon of concentration

quenching, one is multipole-multipole interaction, the other one is exchange interaction. In order to know which one causes the concentration quenching, the critical distance between the neighboring Pr^{3+} ions is obtained by the following equation:

$$R_c \approx 2\times(\frac{3V}{4\pi x_c N})^{\frac{1}{3}} \quad (1)$$

where x_c is the critical concentration, N is the number of center cations in the unit cell, and V is the volume of the unit cell [35] and , the value of V and N are 611.82 $Å^3$ and 2 in the crystal lattice，respectively [28]. Supposed that the critical concentration is 0.02, the critical distance among Pr^{3+} ions is calculated to be 30.81 Å. However, the critical distance of exchange interaction is normally around 5 Å [36], thus the exchange interaction plays little role in the energy transfer among Pr^{3+} ions because R_c is much larger than 5 Å . Therefore, the energy transfer mechanism among Pr^{3+} ions is considered as multipolar interaction. The type of the multipolar interaction can be determined based on the following equation:

$$\frac{I}{x} = K\left[1+\beta(x)^{Q/3}\right]^{-1} \quad (2)$$

Where I presents the integrated emission intensity, x is the concentration of activator, K and β are constants [36]. The Q is the index of electric multipole, for dipole-dipole, dipole-quadrupole, and quadrupole - quadrupole , corresponding to 6, 8, and 10, respectively. Equation (2) can be approximately simplified to be $\lg(\frac{I}{x}) = A - \frac{Q}{3}\lg x$. As inset (b) in Fig. 4 shows, the values of lg(I/x) as a function on the lg(x) are plotted. The nearly liner fitting can be obtained and the slope of the fitting line is about -1.97. So, the value of Q can be calculated to be 5.91, which reveals that the concentration quenching of Pr^{3+} in $La_3GaGe_5O_{16}$ host is mainly due to the dipole-dipole interaction.

3.3 Long persistent properties

To probe the persistent luminescence characteristics, the afterglow spectrum of $La_{2.99}GaGe_5O_{16}$: $0.01Pr^{3+}$, as shown in Fig. 5, was recorded immediately after ceasing the irradiation. $La_{2.99}GaGe_5O_{16}$:$0.01Pr^{3+}$ sample shows a pink persistent emission which is similar in shape and position to the emission spectrum. This indicates that the stored energy gets back to the Pr^{3+} following the same way as the photoluminescence process. The inset in Fig. 5 presents the CIE coordinates (0.416, 0.304) of the afterglow spectrum for $La_{2.99}GaGe_5O_{16}$: $0.01Pr^{3+}$. This novel pink long persistent luminescence from $La_{2.99}GaGe_5O_{16}$: $0.01Pr^{3+}$ can last several minutes after irradiation by UV light.

In order to study the afterglow decay behaviors and the concentration quenching of $La_{3-x}GaGe_5O_{14}$:xPr^{3+} (x = 0.005, 0.01, 0.02 and 0.04) phosphors in detail, the long afterglow decay curves of samples were measured at room temperature. Figure 6(a) gives the persistent luminescence decay curves of $La_{3-x}GaGe_5O_{14}$:xPr^{3+} (x = 0.005, 0.01, 0.02 and 0.04) phosphors after irradiation by a 15 W low-pressure mercury discharge lamp for 3 min. For higher concentration, the persistent emission is too weak to be observed by human naked eyes. To our knowledge, the energy transfer between activators, a principal factor, results in the fluorescence concentration , and requires considerable interaction and energy resonance between activators [37]. However, the concentration quenching of persistent luminescence is attributed to electron transfer between traps or activators by tunneling, which requires wave function overlap and energy resonance [37]. For $La_{3-x}GaGe_5O_{14}$:xPr^{3+}, the width of potential barrier would be effectively reduced along with the increasing concentration of dopant Pr^{3+} . That is to say, the probability of electron tunneling among traps or activators would increase and even the trapped electrons can reach activators easily without heating. From Figure 6(a), we can see that the

quenching of persistent luminescence takes place when the concentration of dopant Pr^{3+} is over 0.01.

As presented in Figure 6(b), the afterglow decay curve of $La_{0.995}GaGe_5O_{14}$:$0.005Pr^{3+}$ is well fitted with the double-exponential function:

$$I(t) = A\exp(-\frac{t}{\tau_1}) + B\exp(-\frac{t}{\tau_2}) \quad (3)$$

where I(t) is the persistent luminescence intensities at times t ; A and B are constants, and τ_1 and τ_2 are the decay times for the short and long decay components, respectively. The other afterglow decay curves are fitted with double-exponential function (1). All the fitting results of all decay curves are listed in table 1. Apparently, the fitting results indicate that there are two decay processes involved in $La_{3-x}GaGe_5O_{14}$:xPr^{3+} (x = 0.005, 0.01, 0.02 and 0.04) including a rapid decay process at first and then a slow decay process.

The persistent luminescence phenomenon is a special case of thermally stimulated luminescence at room temperature . Even though the nature of the defects is still disputed, some properties such as the defect depth and density can be investigated by thermoluminescence (TL) measurements [1, 37]. As a rule, each TL peak stands for a kind of trapping centers and the relative trap density or trapping capacity is roughly proportional to the integral TL intensity.

Figure 7(a) shows the TL curves of $La_{3-x}GaGe_5O_{14}$:xPr^{3+}(x = 0.005, 0.01, 0.02 and 0.04) sample measured immediately after ceasing irradiation for 3 min. It can be seen that the integral TL intensity of $La_{2.99}GaGe_5O_{14}$:$0.01Pr^{3+}$ sample is largest to all appearance. Figure 7(a) can prove the optimal doped concentration for the best long persistent luminescence in $La_{3-x}GaGe_5O_{14}$:xPr^{3+} on the other side. In order to further investigate the TL curve, a detailed analysis of TL curve for $La_{2.99}GaGe_5O_{16}$: $0.01Pr^{3+}$ is deconvoluted by the curve fitting technique based on the Gaussian

equation and a good agreement between experimental and calculated glow curves is obtained in Fig.7(b). At least, two Gaussian peaks (a, and b) are obtained and located at around 357 and 390 K, respectively.

The trap depth and density of TL bands for Pr^{3+} doped $La_3GaGe_5O_{14}$ samples can be calculated based on the following two equations (3) [38].

$$E = 2.52(\frac{k_B T_m^2}{\omega}) - 2k_B T_m \quad (4)$$

where E is the trap depth; k_B is Boltzmann's constant; T_m is the temperature corresponding to the TL glow peak; in which ω is the full width at half maximum of the TL band. The estimated trap depth for these two Gaussian peaks is about 0.71 and 0.78 eV, respectively. In general, the TL peaks, corresponding to the trap depth range of 0.65-0.75 eV, is more suitable to generate optimal long afterglow at room temperature [37]. The low TL band (peak a) is situated close to the ideal temperature for the release at room temperature of the energy stored, while the high one (peak b) can contribute mainly to the energy storage capability of the materials, ensuring the long duration of the persistent luminescence. Hence, $La_{2.99}GaGe_5O_{14}$:$0.01Pr^{3+}$ gives a long persistent luminescence.

3.4 Possible mechanism of long persistent luminescence

In persistent luminescence materials, the storage and release of energy takes place in the the defects of the materials in spite that the nature of the traps is unknown in the afterglow process [39]. In order to fully understand the possible mechanism of long persistent luminescence in the phosphor $La_3GaGe_5O_{14}$:Pr^{3+}, the primary issue is the exploration of trap states and types. Except for the intrinsic traps such as the oxygen vacancy and germanium vacancy, there are two kinds of lattice defects due to the doped ions substituting the cation ions in the host. The praseodymium

ions in $La_3GaGe_5O_{14}$ host are the mixed valence (Pr^{3+}, Pr^{4+}) because the praseodymium ions are from the multivalent oxides Pr_6O_{11}. First, Pr^{3+} ions are easy to substitute for the sites of equivalent La^{3+} ions via the process $Pr^{3+} + La^{3+} \rightarrow Pr_{La^{3+}}^{3+\times}$. It may cause the tiny change in volume due to the unequal ionic radii. The other, two La^{3+} ions can be replaced by two Pr^{4+} ions accompanied by the formation of an interstitial oxygen ($O_i^{2-\prime\prime}$) to maintain electrical neutrality in the form of $[2Pr^{4+} + 2La^{3+} \rightarrow 2Pr_{La^{3+}}^{4+\bullet} + O_i^{2-\prime\prime}]$. It might lead to the formation of a defect cluster $[Pr_{La^{3+}}^{4+\bullet}\text{-}O_i^{2-\prime\prime}\text{-}Pr_{La^{3+}}^{4+\bullet}]$ due to electrostatic interaction. The defects $Pr_{La^{3+}}^{4+\bullet}$ can act as the electron traps while the other defects $O_i^{2-\prime\prime}$ can be regarded as the hole traps.

To understand the dynamical process in persistent luminescence, a schematic graph based on the above results is proposed and illustrated in Figure 8. However, the ground level energies for Pr^{3+} ions in the host band structure of $La_3GaGe_5O_{14}$ are much difficult to obtain. To discuss the afterglow luminescence, just for illustration purpose, the Pr^{3+} energy levels are placed into the middle of the forbidden zone. The relative positions of the traps with respect to the bottom of conduction band can be determined based on the TL peaks. To simplify the description, we assign the shallow trap and deep trap in the afterglow process as the Trap-1 and Trap-2, respectively. After irradiation with the ultraviolet light , the ground electrons of Pr^{3+} are excited along path 1 to the $4f^15d$ state, the latter lying in the conduction band. This leads to a separation of the electrons and holes. Subsequently, holes flow into the valence band, following path 5. The majority of excited electrons will be back to $^3P_2$ level of Pr^{3+} and then relax to $^3P_0$ level in non-radiative way. The subsequent jumping of electrons to the ground levels $^3F_2$ and ^3H_i (i =4, 5 and 6) of Pr^{3+} and recombination of holes lead to the characteristic emission of Pr^{3+} ions (process numbered 5 and 6). These processes present photoluminescence emission of $La_3GaGe_5O_{14}$:Pr^{3+}. However, The

residual minority excited electrons relax to the lower end of the conduction band and then are captured by the different traps (Trap 1 and 2) through the non-radiative path 2. In the initial stage of the afterglow luminescence, the electrons captured by Trap-1 escape thermally via the conduction and are transferred to the activators Pr^{3+} (process numbered 4), followed by the recombination between electrons and holes and resulting in the initial persistent emission. The rapid decay process of the afterglow corresponds to the depletion of Trap-1. Subsequently, the persistent luminescence mainly originates from Trap-2 via quantum tunneling (process 4), giving a weak but long persistent luminescence.

4. Conclusion

This novel $La_3GaGe_5O_{16}:Pr^{3+}$ phosphor is obtained from via the solid state reaction. Firstly, $La_3GaGe_5O_{16}$ host is concluded to a new self-activated luminescent host. The pink long afterglow luminescence from $La_{2.99}GaGe_5O_{16}:0.01Pr^{3+}$ is observed. For $La_{3-x}GaGe_5O_{16}:xPr^{3+}$, the doping concentration of Pr^{3+} has a significant affect on the photoluminescence and long afterglow luminescence. The concentration quenching of Pr^{3+} in $La_3GaGe_5O_{16}:Pr^{3+}$ occurs at a low content due to the dipole-dipole interaction. The mechanisms of the photoluminescence and afterglow phenomenon is proposed based on the experimental results. In addition, further studies to optimize preparation conditions for the optimal intensity and duration of persistent luminescence of this phosphor are under our consideration.

Acknowledgements

This work is supported by the National Natural Science Foundation of China (No. 21471038).

References:

[1] S.W.S. McKeever, Thermoluminescence of Solids, Cambridge University Press, New York

(1985)

[2] G. Blasse, B. C. Grabmaier. Luminescent materials; Berlin : Springer-Verlag, 1994.

[3] F.W. Kang, M.Y. Peng, X.B. Yang, G.P. Dong, G.H. Nie, W. J. Liang, S.H. Xu and J.R. Qiu, J. Mater. Chem. C, 2014, 2, 6068.

[4] F.W. Kang, X.B. Yang, M.Y. Peng, L. Wondraczek, Z. J. Ma, Q.Y. Zhang, and J.R. Qiu, J. Phys. Chem. C, 2014, 118, 7515.

[5] F.W Kang, M.Y. Peng, Q.Y. Zhang and J.R. Qiu, Chem-Eur. J. 2014, 20, 11522.

[6] W M. Yen, S. Shionoya, H. Yamamoto. Practical Applications of phosphors; CRC Press: Baca Raton, FL, 2006.

[7] P F. Smet, D. Poelman, M P. Hehlen, Opt. Mater. Express, 2012, 2, 452.

[8] Z W. Pan, Y Y. Lu, F. Liu, Nat. Mater. 2012, 11, 58.

[9] Y. Li, S. F. Zhou, Y.Y. Li, K. Sharafudeen, Z.J. Ma, G.P. Dong, M.Y. Penga and J.R. Qiu, J. Mater. Chem. C, 2014, 2, 2657.

[10] R. Weissleder, Nat. Biotechnol., 2001, 19, 316.

[11] M. H. Aven and R. M. Potter, J. Electrochem. Soc.,1958, 105, 134.

[12] T. Matsuzawa,Y. Aoki, N. Takeuchi, Y. Murayama, J. Electrochem. Soc., 1996, 143, 2670.

[13] X M.Teng, W D. Zhuang,Y S. Hu, CL. Zhao, J. Alloys. Compd., 2008, 458, 446.

[14] Y. H. Lin, Z. L. Tang, Z.T. Zhang and C.W. Nan, Appl. Phys. Lett. 2002, 81, 996.

[15] B. Liu, C S. Shi, M. Yin, L. Dong, Z G.Xiao, J. Alloys. Compd., 2005, 387, 65.

[16] D D. Jia, W Y. Jia, D R. Evans, W. M. Dennis, H. Liu, J. Zhu and W. M. Yen . J. Appl. Phys., 2000, 88, 3402.

[17] Z. Hong, P. Zhang, X. Fan, M. Wang, J. Lumin. 2007, 124, 127.

[18] F.W. Kang, Y. H. Hu, L. Chen, X.J. Wang, H.Y. Wu, J. Lumin., 2013, 135, 113.

[19] F.W. Kang, Y. H. Hu, H.Y. Wu, Z.F. Mu, G.F. Ju, C.J. Fu, N.N. Li, J. Lumin., 2002, 132, 887.

[20] F. Kang, Y. Hu, L. Chen, X. Wang, Z. Mu, H. Wu, G. Ju, Appl. Phys. B, 2012, 107, 833.

[21] K. Van Den Eeckhout, P. F. Smet, J. Lumin. 2009, 129,1140.

[22] Z. Ju, R. Wei, J. Zheng, X. Gao, S. Zhang, W. Liu, Appl Phys Lett., 2011, 98,121906-3.

[23] Y Q. Li, Y H. Wang, Y. Gong, X H. Xu, M J. Zhou, Opt. Express, 2010,18, 24853.

[24] P T. Diallo, P. Boutinaud, R. Mahiou, J C. Cousseins, Phys Status Solidi A, 1997, 160, 255.

[25] S. Lian, Y. Qi, C. Rong, L. Yu, A.Zhu, D. Yin and S. Liu, J. Phys. Chem. C, 2010, 114, 7196.

[26] P Boutinaud1, L Sarakha and R Mahiou, J. Phys.: Condens. Matter, 2009, 21, 025901

[27] A. Lecointre, A. Bessière, A. J. J. Bos, P. Dorenbos, B. Viana, and S. Jacquart, J. Phys. Chem. C, 2011, 115, 4217.

[28] G.Adiwidjaja, M. Broeker, C. Claus, K. Friese, K.H. Klaska, O. Jarchow, M.Ruks, I.Wozniak, Z. Kristallogr, 1998, 213, 223.

[29] J. Zhou and Z.G. Xia, RSC Adv., 2014,4, 46313.

[30] J. Zhou and Z.G. Xia, J. Mater. Chem. C, 2014, 2, 6978.

[31] Y. Jin, Y. Hu, L. Chen, X. Wang, G. Ju and Z. Mou, J. Am. Ceram. Soc., 2013,96,3821.

[32] M. N. Kabler and D. A. Patterson, Phys. Rev. Lett. 1967, 19, 652.

[33] A. Shluger and E. Stefanovich, Phys. Rev. B, 1990, 42, 9664.

[34] J. F. Meng, B. K. Rai, R. S. Katiyar, and G. T. Zou, Phys. Lett. A, 1997, 229,254–8.

[35] G. Blasse, J. Solid State Chem., 1986, 62, 207.

[36] D. L. Dexter, J. Chem. Phys., 21:836-840(1953).

[37] G. Blasse,B. C. Grabmaier. Luminescent materials; Berlin : Springer-Verlag, 1994.

[38] R. Chen, J. Electrochem. Soc., 1969, 116, 1254.

[39] Y. Jin, Y. Hu, L. Chen, X. Wang, Z. Mu, G. Ju. Mater. Lett. 2014, 126, 75.

Figure captions

Figure 1 powder XRD patterns of the sample $La_3GaGe_5O_{16}$ host and $La_{3-x}GaGe_5O_{16}$: $x$$Pr^{3+}$($x$= 0.01, 0.02 and 0.04) samples

Figure 2 (a) Diffuse reflection spectra of pure $La_3GaGe_5O_{16}$ and $La_3GaGe_5O_{16}$:0.01Pr^{3+} at room temperature; (b) excitation and emission spectra of $La_3GaGe_5O_{16}$ host

Figure 3 (a) Excitation spectrum (λ_{em}=612 nm) and (b) emission spectrum (λ_{ex}=282 nm) of $La_{2.99}GaGe_5O_{16}$: 0.01Pr^{3+} sample at room temperature

Figure 4 the emission spectra of $La_{3-x}GaGe_5O_{16}$:$x$$Pr^{3+}$ (x=0.005, 0.01, 0.02, 0.04 and 0.06); inset (a) the integrated intensity of Pr^{3+} as a function of its doping concentrations; inset (b) the dependence of lg(I/x) on lg(x) based on equation (2)

Figure 5 the afterglow spectrum of $La_{2.99}GaGe_5O_{16}$: 0.01Pr^{3+}; Inset: The CIE coordinates of the afterglow spectrum for $La_{2.99}GaGe_5O_{16}$: 0.01Pr^{3+}

Figure 6(a) the long afterglow decay curves of $La_{3-x}GaGe_5O_{16}$: $x$$Pr^{3+}$ (x = 0.005, 0.01, 0.02 and 0.04); **(b)** the afterglow decay curve of $La_{2.99}GaGe_5O_{16}$: 0.01Pr^{3+} with its fitting result.

Figure 7(a) the thermoluminescence (TL) glow curve of $La_{3-x}GaGe_5O_{16}$: $x$$Pr^{3+}$ (x = 0.005, 0.01, 0.02 and 0.04) at waiting time of 3 min after the removal of excitation; **(b)** the TL glow curve of $La_{2.99}GaGe_5O_{16}$: 0.01Pr^{3+} with three Gaussian peaks (a, b, and c).

Figure 8 the schematic diagram of the phosphorescence mechanism in $La_3GaGe_5O_{14}$:Pr^{3+}. (• represents electrons and ○ refers holes; dotted arrow shows carrier relaxation or thermal motion)

Table 1 Decay times for two exponential components of $La_{3-x}GaGe_5O_{16}$:xPr^{3+} (x = 0.005, 0.01, 0.02, and 0.04)

Contents of Pr^{3+} ions	τ_1(s)	I_1	τ_2(s)	I_2	R^2
0.005	36.61	688314	110.28	468983	0.9999
0.01	51.40	908692	124.57	558522	0.9999
0.02	36.86	548425	111.23	442751	0.9999
0.04	34.43	192322	105.94	81613	0.9999

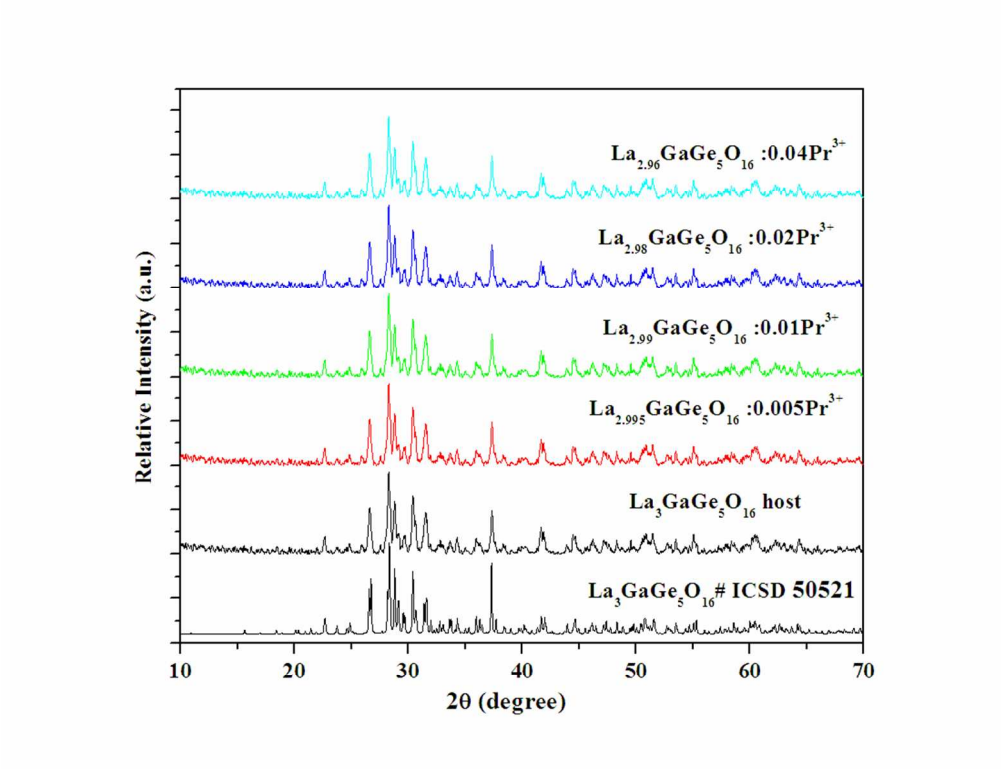

Figure 1 powder XRD patterns of the sample La3GaGe5O16 host and La3-xGaGe5O16: xPr3+(x= 0.01, 0.02 and 0.04) samples
186x143mm (150 x 150 DPI)

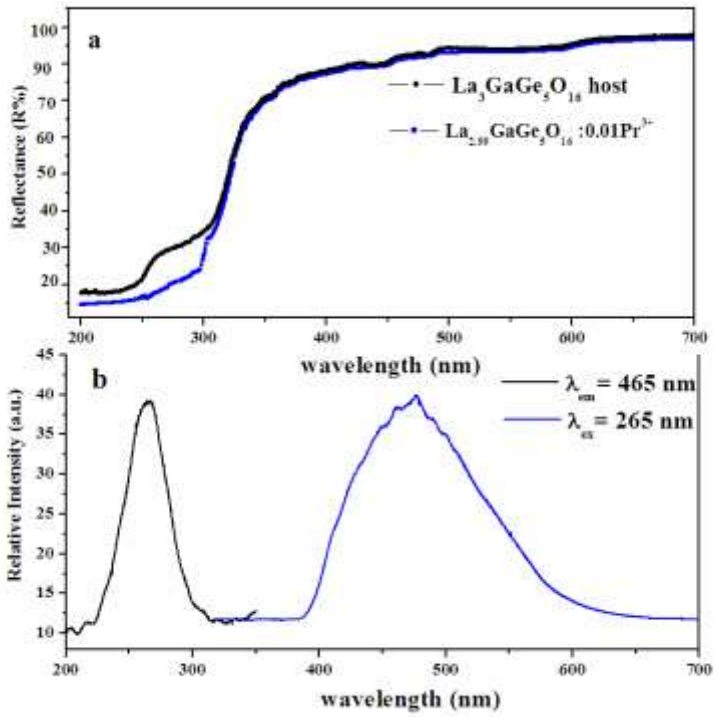

Figure 2 (a) Diffuse reflection spectra of pure La3GaGe5O16 and La3GaGe5O16:0.01Pr3+ at room temperature; (b) excitation and emission spectra of La3GaGe5O16 host
186x143mm (150 x 150 DPI)

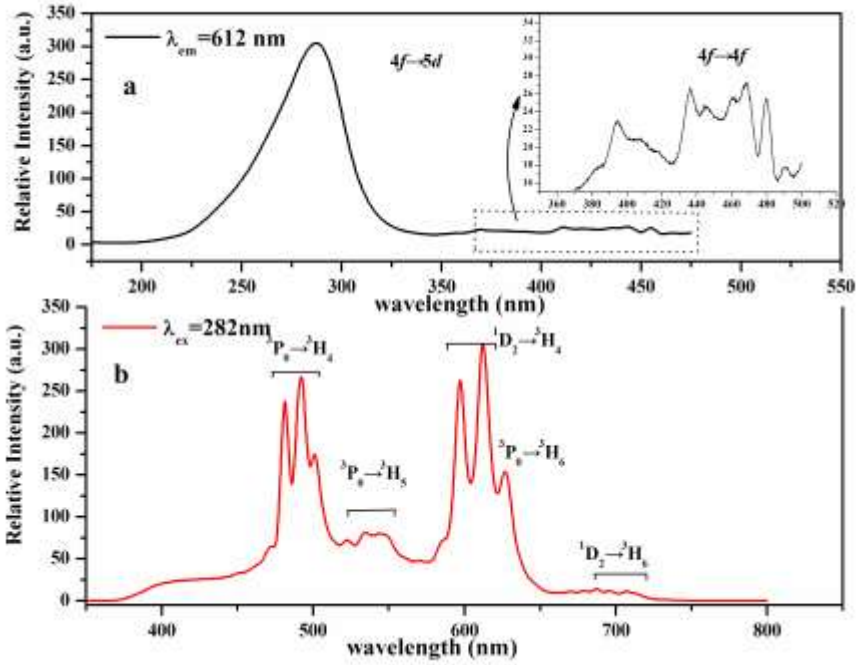

Figure 3 (a) Excitation spectrum (λem=612 nm) and (b) emission spectrum (λex=282 nm) of La2.99GaGe5O16: 0.01Pr3+ sample at room temperature
594x420mm (150 x 150 DPI)

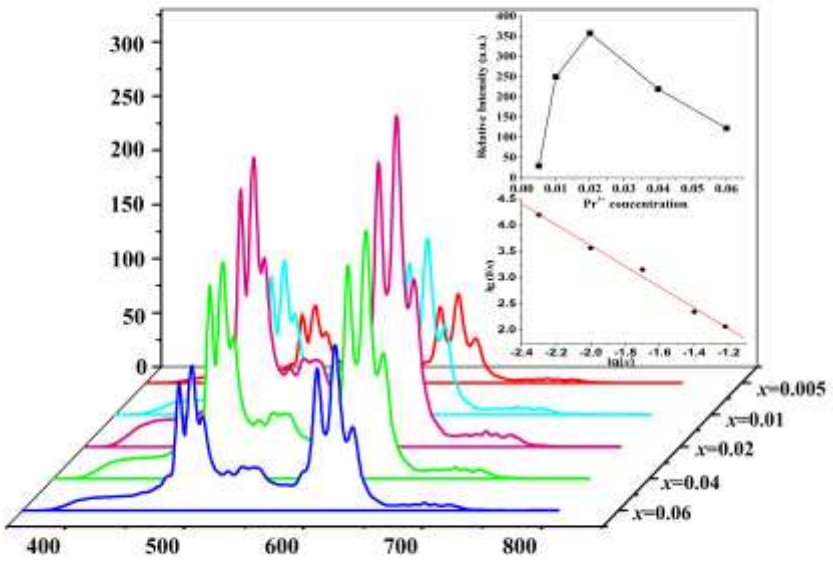

Figure 4 the emission spectra of La3-xGaGe5O16:xPr3+ (x=0.005, 0.01, 0.02, 0.04 and 0.06); inset (a) the integrated intensity of Pr3+ as a function of its doping concentrations; inset (b) the dependence of lg(I/x) on lg(x) based on equation (2)
1117x863mm (150 x 150 DPI)

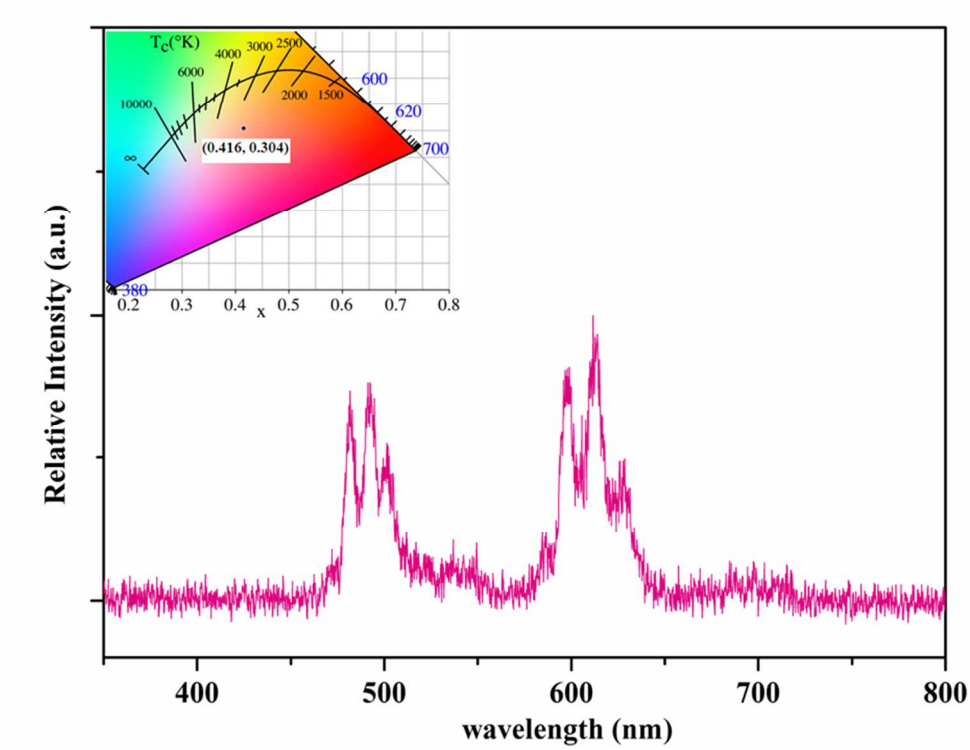

Figure 5 the afterglow spectrum of La2.99GaGe5O16: 0.01Pr3+; Inset: The CIE coordinates of the afterglow spectrum for La2.99GaGe5O16: 0.01Pr3+
254x190mm (96 x 96 DPI)

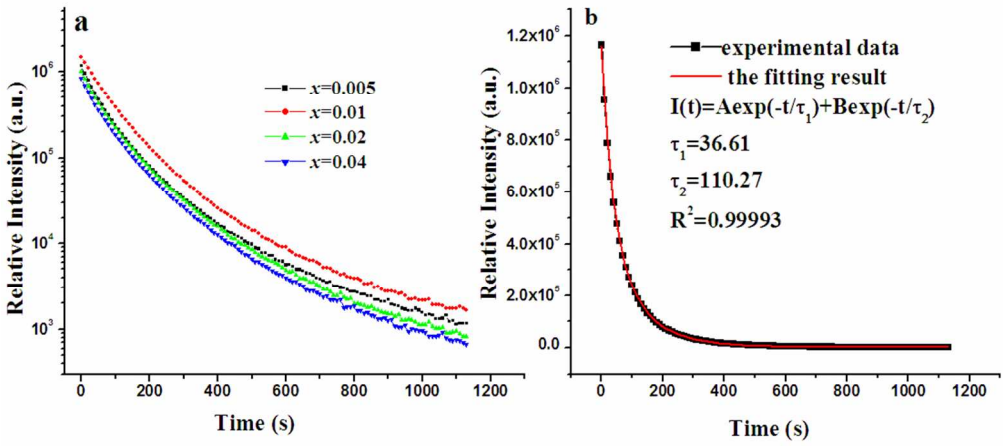

Figure 6(a) the long afterglow decay curves of La3-xGaGe5O16: xPr3+ (x = 0.005, 0.01, 0.02 and 0.04); (b) the afterglow decay curve of La2.99GaGe5O16: 0.01Pr3+ with its fitting result .
186x143mm (150 x 150 DPI)

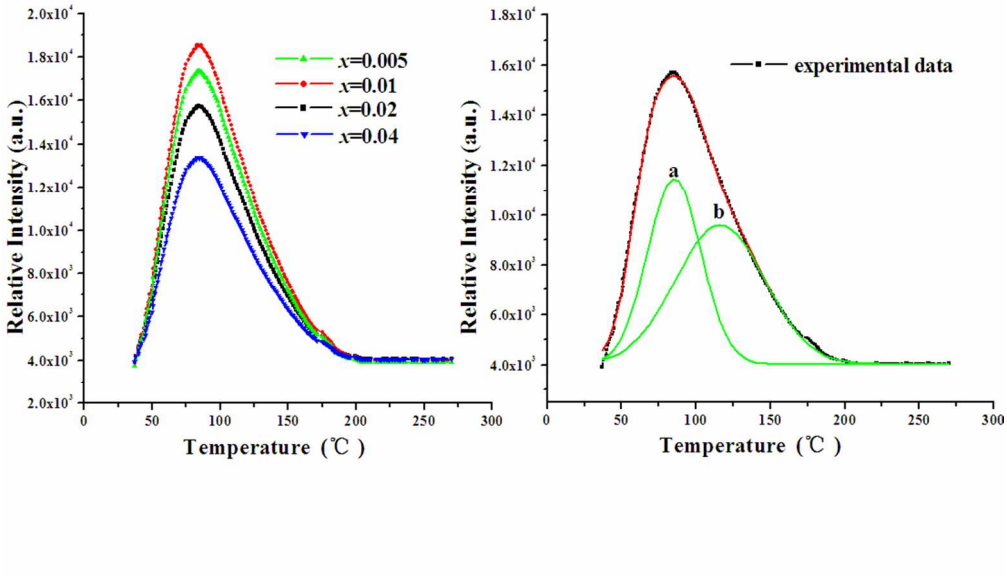

Figure 7(a) the thermoluminescence (TL) glow curve of La3-xGaGe5O16: xPr3+ (x = 0.005, 0.01, 0.02 and 0.04) at waiting time of 3 min after the removal of excitation; (b) the TL glow curve of La2.99GaGe5O16: 0.01Pr3+ with three Gaussian peaks (a, b, and c).
186x143mm (150 x 150 DPI)

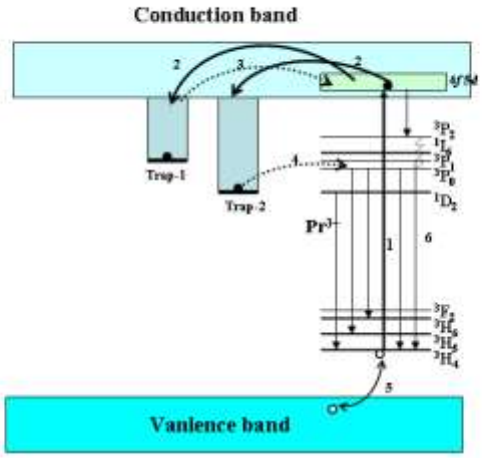

Figure 8 the schematic diagram of the phosphorescence mechanism in La3GaGe5O14:Pr3+. (• represents electrons and ○ refers holes; dotted arrow shows carrier relaxation or thermal motion)
254x190mm (96 x 96 DPI)